

## Temperature anisotropy at equilibrium reveals nonlocal entropic contributions to interfacial properties

Øivind Wilhelmsen\*


*Department of Energy and Process Technology, Norwegian University of Science and Technology, NO-7491 Trondheim, Norway  
and SINTEF Energy Research, NO-7465 Trondheim, Norway*

Thuat T. Trinh

*Department of Civil and Environmental Engineering, Norwegian University of Science and Technology, NO-7491 Trondheim, Norway*

Anders Lervik

*Department of Chemistry, Norwegian University of Science and Technology, NO-7491 Trondheim, Norway*

 (Received 14 December 2015; revised manuscript received 20 December 2017; published 18 January 2018)

Density gradient theory for fluids has played a key role in the study of interfacial phenomena for a century. In this work, we revisit its fundamentals by examining the vapor-liquid interface of argon, represented by the cut and shifted Lennard-Jones fluid. The starting point has traditionally been a Helmholtz energy functional using mass densities as arguments. By using rather the internal energy as starting point and including the entropy density as an additional argument, following thereby the phenomenological approach from classical thermodynamics, the extended theory suggests that the configurational part of the temperature has different contributions from the parallel and perpendicular directions at the interface, even at equilibrium. We find a similar anisotropy by examining the configurational temperature in molecular dynamics simulations and obtain a qualitative agreement between theory and simulations. The extended theory shows that the temperature anisotropy originates in nonlocal entropic contributions, which are currently missing from the classical theory. The nonlocal entropic contributions discussed in this work are likely to play a role in the description of both equilibrium and nonequilibrium properties of interfaces. At equilibrium, they influence the temperature- and curvature-dependence of the surface tension. Across the vapor-liquid interface of the Lennard Jones fluid, we find that the maximum in the temperature anisotropy coincides precisely with the maximum in the thermal resistivity relative to the equimolar surface, where the integral of the thermal resistivity gives the Kapitza resistance. This links the temperature anisotropy at equilibrium to the Kapitza resistance of the vapor-liquid interface at nonequilibrium.

DOI: [10.1103/PhysRevE.97.012126](https://doi.org/10.1103/PhysRevE.97.012126)

### I. INTRODUCTION

In the narrow interfacial region, properties change dramatically in only a few nanometers. Interfacial properties are crucial for a wide variety of phenomena, ranging from DNA replication [1] to volcano eruptions [2] and weather forecasts [3]. The time-average local structure of interfaces can be described by classical density functional theory for fluids, which has played a key role in the study of interfacial phenomena for more than a century [4,5]. The first approximation to classical density functional theory is called density gradient theory or square gradient theory (SGT). Such theories have provided insight into how the surface tension of fluids depends on temperature, curvature, and composition [6–8]. They have also been used to study nonequilibrium properties of interfaces such as the temperature- and curvature-dependence of the interface transfer coefficients [9–12].

There is still a disagreement between the theoretical predictions from classical density functional theory and experimental values for the surface tension. This discrepancy has

been attributed to temperature-dependent influence parameters [13] or to capillary waves [14]. In this work we will show, by an extension of SGT, how the classical expression for the surface tension is missing terms originating in nonlocal entropic contributions. These contributions could influence both the temperature- and curvature-dependence of the surface tension and may account for part of the discrepancy between experiments and theory.

The extended theory presented in this work suggests that the configurational part of the temperature has anisotropic contributions across the interface, even under equilibrium conditions. Even though temperature is a familiar concept to most, it is debated in the literature [15–27]. Frequent discussions debate whether the temperature of a nucleating cluster is higher or lower than the temperature of the surrounding vapor [25–27], or if the temperature of an imploding bubble can become sufficiently high to trigger thermonuclear fusion [21–23]. Further progress on these topics requires the temperature to be properly understood in highly heterogeneous systems such as at interfaces. We test our extension of SGT by performing molecular dynamics (MD) simulations and find a temperature anisotropy that agrees qualitatively with the theoretical predictions.

\*oivind.wilhelmsen@ntnu.no

The results from our simulations also indicate a surprising link between the anisotropy in the configurational temperature in *equilibrium* simulations and the Kapitza resistance, which quantifies the interfacial resistance to heat transfer under *nonequilibrium* conditions [28–33]. For solid-solid and solid-liquid interfaces, the Kapitza resistance has been described theoretically in terms of the acoustic and diffuse mismatch models [34]. For the vapor-liquid interface, however, the Kapitza resistance remains poorly understood, despite its importance in evaporation and condensation [35]. For instance, according to kinetic gas theory [35], the Kapitza resistance gives a temperature-jump that is located in the so-called “Knudsen layer.” Kinetic gas theory correctly predicts that the temperature-jump is at the vapor-side of the interface; however, the predicted magnitudes are far from the values found in experiments or simulations, even for simple fluids [20,36]. Moreover, while nonequilibrium molecular dynamics simulations show that the layer containing the temperature-jump decreases in size with decreasing temperature, kinetic gas theory predicts the opposite behavior [35,37].

Obtaining the Kapitza resistance with SGT requires today a semiempirical fit of the local thermal resistivity function by utilizing results from nonequilibrium molecular dynamics simulations [11,37]. In this work, we connect the temperature jump at nonequilibrium to *equilibrium properties* of the interface. This sheds new light on the origin of the Kapitza resistance of the vapor-liquid interface and may reveal a route for further development of density functional theory for fluids to make the theory predictive, not only for the surface tension, but also for the transport properties of the interface such as the Kapitza resistance.

The paper will be structured as follows. In Sec. II, we revisit the fundamentals of density gradient theory and elaborate why the classical theory is missing nonlocal entropic contributions. It will also be explained why these are expected to result in anisotropic contributions to the configurational temperature across interfaces. We give in Sec. III the technical details about our MD simulations. In Sec. IV we present the results, where we show that the nonlocal entropic contributions that are currently missing from the classical theory play a role in the description of both equilibrium and nonequilibrium interfacial properties. We shall demonstrate how a closer investigation of the configurational temperature can be used to elucidate a part of the interfacial structure that has hitherto remained hidden. Eventually, concluding remarks are given in Sec. V.

## II. THEORY

In this section, we shall revisit the fundamentals of square gradient theory (SGT). We expect the general arguments particularized for SGT to apply also to more sophisticated variants of density functional theory. SGT is capable of reproducing results from MD simulations to a good accuracy for many fluids. In fact, for the particular fluid we consider in this work (argon/Lennard Jones fluid), the SGT approximation gives results which rival those from more sophisticated formulations (see, for instance, Refs. [5,38]). Rather than using the Helmholtz energy as starting point like in the classical theory [39,40], we shall in Sec. II A use the internal energy as starting point and introduce the entropy density as additional variable. In Sec. II B,

we elaborate why the extended theory suggests that the configurational part of the temperature has anisotropic contributions across the interface. Moreover, we show how the validity of the theory can be evaluated by analyzing the kinetic and configurational temperatures in molecular dynamics simulations.

### A. Introducing the entropy density as a variable in the thermodynamic description of interfaces

In homogeneous systems, classical thermodynamics states that the internal energy density of a fluid is a function of the mass densities and the entropy density [41]. On the contrary, density functional theory for fluids has been based on functional derivatives with respect to only mass densities for the last century, following van der Waal’s pioneering work on the topic [4,39,42–44]. The main justification for using the Helmholtz energy as starting point is that the temperature and mass densities are then canonical variables [41]. Since the temperature is constant in space at equilibrium, only the mass densities are relevant variables.

In this work, we follow the phenomenological approach from classical thermodynamics and use rather the internal energy as starting point. By properly Legendre transforming the internal energy functional, we will demonstrate that the Legendre transform of the internal energy to the Helmholtz energy does not remove the entropic contributions with a non-local dependence. Therefore, part of the information about the structure of the interface, which in Sec. IV will be elucidated with MD simulations, will be lost if the Helmholtz energy is used as starting point.

#### 1. A thermodynamic framework decomposed into kinetic and configurational variables

The Hamiltonian of a classical fluid with  $N$  particles can be written as

$$H(\mathbf{\Gamma}) = \mathcal{K}(p_1, \dots, p_{3N}) + \mathcal{V}(q_1, \dots, q_{3N}), \quad (1)$$

where  $\mathbf{\Gamma} = (p_1, \dots, p_{3N}, q_1, \dots, q_{3N})$  is the phase-space vector with boldface symbols referring to vector quantities,  $q_i$  and  $p_i$  are the generalized coordinates and momenta,  $\mathcal{K}$  is the kinetic energy, and  $\mathcal{V}$  is the potential energy of the fluid. In the following, we shall decompose some of the thermodynamic variables into their kinetic and configurational contributions. A contribution is defined to be kinetic if it depends only on the generalized momenta and configurational if it depends only on the generalized coordinates. In the canonical ensemble, statistical mechanics gives that the internal energy density of a uniform fluid (subscript 0) can be written as [45,46]

$$u_0 = \underbrace{-\left(\frac{\ln(Z_{0(k)})}{\beta V}\right) + T \left(\frac{\partial}{\partial T} \left(\frac{\ln(Z_{0(k)})}{\beta V}\right)\right)}_{u_{0(k)}} + \underbrace{-\left(\frac{\ln(Z_{0(c)})}{\beta V}\right) + T \left(\frac{\partial}{\partial T} \left(\frac{\ln(Z_{0(c)})}{\beta V}\right)\right)}_{u_{0(c)}}, \quad (2)$$

where subscripts “k” and “c” refer to the kinetic and configurational contributions,  $Z$  is the partition function in the canonical ensemble,  $T$  is the temperature,  $s$  is the entropy density, and  $V$  the total volume. Furthermore,

$$\beta = \frac{1}{k_B T}, \quad (3)$$

$$Z_{0(k)} = \frac{1}{h^{3N} N!} \int e^{-\beta \mathcal{K}} dp_1 \dots dp_{3N}, \quad (4)$$

$$Z_{0(c)} = \int e^{-\beta \mathcal{V}} dq_1 \dots dq_{3N}, \quad (5)$$

where  $k_B$  is Boltzmann’s constant and  $h$  is Planck’s constant. Here, it has been used that  $Z$  is the product between the kinetic and configurational partition functions,  $Z_{0(k)}$  and  $Z_{0(c)}$ . Equation (2) shows that in the canonical ensemble, it is possible to decompose the internal energy density  $u_0 = u_{0(k)} + u_{0(c)}$  and the entropy density  $s = s_k + s_c$  into their kinetic and configurational contributions, where  $u_0(\rho, s_{(k)}, s_{(c)})$ ,  $u_{0(k)}(\rho, s_{(k)})$ , and  $u_{0(c)}(\rho, s_{(c)})$  for a single-component fluid, with  $\rho$  being the mass density.

## 2. Extended square gradient theory

Cahn and Hilliard explained why the local argument of the energy functional of a heterogeneous system to a first approximation should contain terms with density gradients squared [47]. Following Rowlinson and Widom [4], we include also the entropy density,  $s$ , as a variable in the internal energy functional of SGT:

$$\begin{aligned} & \bar{U}[s_k(\mathbf{r}), s_c(\mathbf{r}), \rho(\mathbf{r})] \\ &= \int_V d\mathbf{r} u_{\text{sgt}}(\mathbf{r}) \\ &= \int_V d\mathbf{r} [u_{0(k)}(s_k(\mathbf{r}), \rho(\mathbf{r})) + u_{0(c)}(s_c(\mathbf{r}), \rho(\mathbf{r})) \\ & \quad + \kappa_{\rho s} \nabla \rho(\mathbf{r}) \cdot \nabla s_c(\mathbf{r}) + 0.5 \kappa_{\rho} |\nabla \rho(\mathbf{r})|^2 \\ & \quad + 0.5 \kappa_s |\nabla s_c(\mathbf{r})|^2], \end{aligned} \quad (6)$$

where  $\mathbf{r}$  the position vector. We shall hereby refer to this formalism as *extended SGT*. The influence parameters  $\kappa_{\rho}$ ,  $\kappa_{\rho s}$ ,  $\kappa_s$  can in principle depend also on the densities ( $s$  and  $\rho$ ), but we have in this work kept them constant as a first approximation.

The gradient terms represent nonlocal contributions to the energy functional. We have in Eq. (6) decomposed the internal energy density and the entropy density into their kinetic and configurational parts, in accordance with the discussion in Sec. II A 1. In a homogeneous system, this decomposition is unnecessary. The argument for decomposition of these variables in a heterogeneous system is that the kinetic part of the Hamiltonian,  $\mathcal{K}$ , is strictly local because it only involves particle momenta. Therefore, only the configurational part of the entropy density should give nonlocal gradient contributions in the extended SGT framework.

In the canonical ensemble, i.e., at fixed temperature,  $T$ , volume  $V$ , and number of particles  $N$ , equilibrium is characterized by a constrained minimum in the Helmholtz energy, which results from Legendre transforming the internal energy [41].

This corresponds to

$$\delta A = \delta \bar{U} - T \delta \int_V d\mathbf{r} s(\mathbf{r}) - \lambda \delta \int_V d\mathbf{r} \rho(\mathbf{r}) = 0, \quad (7)$$

where the last term on the right-hand side takes into account the fixed total number of particles and  $\lambda$  is a Lagrange multiplier. The necessary conditions for a minimum are given by the Euler-Lagrange equations:

$$T = T_{\text{sgt}(k)} = \frac{\partial u_{0(k)}(\mathbf{r})}{\partial s_k(\mathbf{r})}, \quad (8)$$

$$T = T_{\text{sgt}(c)} = \frac{\partial u_{0(c)}(\mathbf{r})}{\partial s_c(\mathbf{r})} - \kappa_s \nabla^2 s_c(\mathbf{r}) - \kappa_{\rho s} \nabla^2 \rho(\mathbf{r}), \quad (9)$$

$$\mu = \mu_{\text{sgt}} = \frac{\partial u_0(\mathbf{r})}{\partial \rho(\mathbf{r})} - \kappa_{\rho s} \nabla^2 s_c(\mathbf{r}) - \kappa_{\rho} \nabla^2 \rho(\mathbf{r}), \quad (10)$$

where we have added the subscripts “k” and “c” to the temperatures in Eqs. (8) and (9), since they are based only on the kinetic and the configurational part of the Hamiltonian, respectively. Furthermore, we identify the Lagrange multiplier to be the chemical potential,  $\lambda = \mu$ . The present framework differs from the traditional approach mainly by using the internal energy as starting point rather than the Helmholtz energy [39,41]. It is evident from Eq. (7) that the Legendre transform  $-T \delta \int_V d\mathbf{r} s(\mathbf{r})$  keeps the nonlocal entropic contributions of the functional unchanged, just like the term  $-\mu \delta \int_V d\mathbf{r} \rho(\mathbf{r})$  conserves the nonlocal dependence with respect to  $\rho$  in the classical theory. We define the scalar pressure as

$$\begin{aligned} p_{\text{sgt}}(\mathbf{r}) &= -u_{\text{sgt}}(\mathbf{r}) + s_k(\mathbf{r}) T_{\text{sgt}(k)} \\ & \quad + s_c(\mathbf{r}) T_{\text{sgt}(c)} + \rho(\mathbf{r}) \mu_{\text{sgt}}. \end{aligned} \quad (11)$$

At equilibrium, the momentum balance gives

$$\nabla p_{\text{sgt}}(\mathbf{r}) + \nabla \cdot \boldsymbol{\sigma}(\mathbf{r}) = 0, \quad (12)$$

where  $\boldsymbol{\sigma}$  is the tension tensor. We further determine  $\boldsymbol{\sigma}$  by following a similar procedure as Yang *et al.* [48]: Equation (8) was multiplied with  $\nabla s_k$ , Eq. (9) with  $\nabla s_c$ , Eq. (10) with  $\nabla \rho$  and the sum was taken. By using Eq. (11) and tensor algebra, the gradient  $\nabla p_{\text{sgt}}$  can be separated out and the tension tensor can be determined by use of Eq. (12):

$$\begin{aligned} \boldsymbol{\sigma}(\mathbf{r}) &= \kappa_{\rho} \nabla \rho(\mathbf{r}) \nabla \rho(\mathbf{r}) \\ & \quad + 2 \kappa_{\rho s} \nabla \rho(\mathbf{r}) \nabla s_c(\mathbf{r}) + \kappa_s \nabla s_c(\mathbf{r}) \nabla s_c(\mathbf{r}). \end{aligned} \quad (13)$$

The expression in Eq. (13) reproduces the tension tensor from classical SGT with  $\kappa_{\rho s} = 0$  and  $\kappa_s = 0$ . For the planar interface, we can now evaluate the pressure tensor, where the parallel and perpendicular components of the pressure tensor are

$$p_{\parallel}(z) = p_{\text{sgt}}(z), \quad (14)$$

$$p_{\perp}(z) = p_{\text{sgt}}(z) + \sigma_{zz}(z), \quad (15)$$

and the surface tension is

$$\gamma = \int_{-\infty}^{\infty} dz [p_{\perp}(z) - p_{\parallel}(z)] = \int_{-\infty}^{\infty} dz [\sigma_{zz}(z)], \quad (16)$$

where  $z$  is the direction perpendicular to the interface. The terms in Eq. (13) with gradients of the configurational entropy

density represent new contributions to the surface tension that are missing from the classical theory. They are of a different origin and have a different behavior than the first term on the right-hand side of Eq. (13) used in classical SGT.

### B. A theoretical justification for a temperature with anisotropic spatial contributions in heterogeneous systems

We shall next particularize to the planar interface, where  $(x, y \in \parallel)$  are the directions parallel and  $(z \in \perp)$  is the direction perpendicular to the interface. In this system, properties such as the densities and the parallel component of the pressure tensor vary only in the direction perpendicular to the interface, i.e., in the  $z$  direction. At every position  $z$ , we assume that the scalar temperature,  $T(z)$ , can be decomposed into independent contributions,  $\xi_x, \xi_y, \xi_z$ , from the  $x, y, z$  directions, respectively, where

$$T(z) = \xi_x(z) + \xi_y(z) + \xi_z(z). \quad (17)$$

A closer inspection of the contributions  $\xi_x(z), \xi_y(z), \xi_z(z)$  from theory and simulations can be used as a route to evaluate the influence of nonlocal entropic contributions on interfacial properties. We discuss the predictions from the extended SGT in Sec. II B 1 and how these predictions can be tested with MD simulations in Sec. II B 2.

#### 1. Spatial contributions to the temperature in square gradient theory

A key assumption in SGT is that the terms and properties that depend only on local variables behave like in a homogeneous fluid (subscript 0) and can thus be represented by an equation of state. It is clear that  $\xi_x = \xi_y = \xi_z$  in the bulk of a homogeneous fluid at equilibrium. By using this same assumption, we find that the first term on the right-hand sides of Eqs. (8) and (9) receives the same contribution from all directions since it is local. The gradient terms on the other hand, contribute only along the direction of the gradient, i.e., perpendicular to the interface. This means that for  $T_{\text{sgt}(k)}$ , the extended SGT formulation presented in Sec. II A suggests that

$$\xi_{\text{sgt}(k),\parallel}(z) = \xi_{\text{sgt}(k),\perp}(z) = \frac{1}{3} \frac{\partial u_{0(k)}(z)}{\partial s_k(z)}, \quad (18)$$

i.e., that there is no anisotropy in the contributions to the kinetic part of the temperature. For  $T_{\text{sgt}(c)}$  on the other hand, the extended SGT formalism suggests that

$$\begin{aligned} \xi_{\text{sgt}(c),\parallel}(z) &= \frac{1}{3} \frac{\partial u_{0(c)}(z)}{\partial s_c(z)}, \\ \xi_{\text{sgt}(c),\perp}(z) &= \frac{1}{3} \frac{\partial u_{0(c)}(z)}{\partial s_c(z)} \\ &\quad - \kappa_s \frac{\partial^2 s_c(z)}{\partial z^2} - \kappa_{\rho s} \frac{\partial^2 \rho(z)}{\partial z^2}, \end{aligned} \quad (19)$$

where the extra terms in Eq. (20) are consequences of including the entropy density as a variable in the thermodynamic description [see Eq. (9)].

#### 2. Spatial contributions to the temperature in molecular simulations

Molecular dynamics simulations give the possibility to independently evaluate the contributions in Eq. (17) from information about the particle momenta as well as the particle interaction forces. Jepps *et al.* proved that the relation [49]

$$\frac{1}{k_B T} = \frac{\langle \nabla_{\Gamma} \cdot \mathbf{B}(\Gamma) \rangle}{\langle \nabla_{\Gamma} H(\Gamma) \cdot \mathbf{B}(\Gamma) \rangle}, \quad (21)$$

could be used to generate microscopic expressions for the temperature by using an arbitrary vector field,  $\mathbf{B}$ . Here,  $\langle \cdot \rangle$  represents the time average in MD simulations and we define the phase space derivative:  $\nabla_{\Gamma} \equiv (\gamma_p \frac{\partial}{\partial p_1}, \dots, \gamma_p \frac{\partial}{\partial p_{3N}}, \gamma_q \frac{\partial}{\partial q_1}, \dots, \gamma_q \frac{\partial}{\partial q_{3N}})$ . Following Morriss and Rondoni [15], we have multiplied the components of  $\nabla_{\Gamma}$ , operating on the generalized momenta and coordinates, with  $\gamma_p$  and  $\gamma_q$  respectively to make it dimensionless. The information contained in the Hamiltonian of the fluid [Eq. (1)] consists of a kinetic part ( $\mathcal{K}$ ) and a configurational part ( $\mathcal{V}$ ). Using  $\mathbf{B}(\Gamma) = \nabla_{\Gamma} \mathcal{K}$  in Eq. (21), we obtain the standard kinetic temperature:

$$T_{\text{md}(k)}(z) = \frac{\overbrace{\left\langle \sum_{i \in \Omega_z} \frac{p_{i,x}^2}{m_i} \right\rangle}^{\xi_{\text{md}(k),\parallel}} + \overbrace{\left\langle \sum_{i \in \Omega_z} \frac{p_{i,y}^2}{m_i} \right\rangle}^{\xi_{\text{md}(k),\parallel}} + \overbrace{\left\langle \sum_{i \in \Omega_z} \frac{p_{i,z}^2}{m_i} \right\rangle}^{\xi_{\text{md}(k),\perp}}}{k_B N_f(\Omega_z)}, \quad (22)$$

which represents the most common way of obtaining the temperature in equilibrium and nonequilibrium MD simulations. If we use the remaining part of the Hamiltonian as generating vector field in Eq. (21), i.e.,  $\mathbf{B}(\Gamma) = \nabla_{\Gamma} \mathcal{V}$ , we obtain the configurational temperature:

$$T_{\text{md}(c)}(z) = \frac{\overbrace{\left\langle \sum_{i \in \Omega_z} F_{i,x}^2 \right\rangle}^{\xi_{\text{md}(c),\parallel}} + \overbrace{\left\langle \sum_{i \in \Omega_z} F_{i,y}^2 \right\rangle}^{\xi_{\text{md}(c),\parallel}} + \overbrace{\left\langle \sum_{i \in \Omega_z} F_{i,z}^2 \right\rangle}^{\xi_{\text{md}(c),\perp}}}{k_B \left\langle - \sum_{i \in \Omega_z} \nabla_i \cdot \mathbf{F}_i \right\rangle}. \quad (23)$$

The terms in the numerators of Eqs. (22) and (23) represent independent contributions from each spatial direction,  $N_f$  is the kinetic degrees of freedom,  $p_{i,j}$  the momentum of particle  $i$  in the  $j$  direction,  $m_i$  the particle mass, and  $\mathbf{F}_i = -\nabla \mathcal{V}$  is the force acting on the particle. Further,  $i \in \Omega_z$  means that the sum only includes atoms within a volume element,  $\Omega_z$  around a position  $z$ .

In previous work, it has been found that Eqs. (22) and (23) are equally applicable for obtaining the local temperature,  $T(z)$ , in steady-state MD simulations, even under nonequilibrium conditions [50,51], given that the discontinuity in the derivatives of the interaction potential is handled properly, by using a sufficiently long truncation distance or tail corrections [52]. Similar to Eq. (8) from the extended SGT, the temperature in Eq. (22) is based only on the kinetic part of the Hamiltonian. Equivalently, the temperatures in Eqs. (9) and (23) are both based only on the configurational part of the Hamiltonian. This suggests that by evaluating the contributions  $\xi_{\text{md},\parallel}(z)$  and  $\xi_{\text{md},\perp}(z)$  in MD simulations, one can assess whether the theoretical predictions from the extended SGT presented in Eqs. (8)

and (9) and in Eqs. (18)–(20) make any sense, and possibly also reveal the presence of nonlocal entropic contributions, since the difference between the spatial temperature contributions across an interface can be explained on the basis of nonlocal entropic contributions.

### III. SIMULATION DETAILS

The vapor-liquid interface of argon as described by the cut and shifted Lennard-Jones (LJ) fluid will be used as an example in this work. This is because of its relative simplicity and since argon (the LJ-fluid) is a popular fluid in simulations and experiments. All simulations in this work were performed with the LAMMPS software package [53]. Argon was modeled with the truncated and shifted LJ potential with a well depth of  $\epsilon/k_B = 119.8$  K, a molecular diameter of  $d = 0.3405$  nm, and a truncation distance of  $4d$  [54]. For completeness, we shall also list the scaled temperature used in the simulations,  $T^* = k_B T/\epsilon$ , where superscript  $*$  refers to scaled variables. The truncation distance was set according to the recommendations in Ref. [50] and we calculated the configurational temperature as prescribed in the same reference. All simulations were performed with periodic boundaries and we used the velocity Verlet integrator with a step size of 0.002 in reduced time units. Liquid-vapor simulations were set up by initiating the argon particles on a regular fcc lattice with a number density equal to 0.8. The simulation cell was then expanded in the  $z$  direction to give a rectangular simulation box with the particles in the center, surrounded by vacuum. This system was equilibrated for  $2 \times 10^7$  time steps with a thermostat (Langevin or Nose-Hoover). This allowed particles to evaporate, resulting in a liquid-vapor system with a uniform temperature and steady density profile. The resulting system was used as a starting point for further investigations.

#### A. Equilibrium NVE simulations

For the equilibrium simulations with constant total energy and volume, we used  $10^6$  particles (unless otherwise specified) in a rectangular simulation volume with dimensions  $\{L_x, L_y, L_z\} = \{106d, 106d, 213d\}$ , where the liquid phase was located in the middle with vapor phases on each side. When larger cross sectional areas were considered,  $L_x$  and  $L_y$  were increased by equal amounts while  $L_z$  was kept unchanged. After equilibration as described above, we simulated the system for  $10^6$  time steps and calculated a local temperature in bins along the  $z$ -direction of the simulation volume as described in details in Ref. [50]. The pressure tensor across the interface, was calculated as described in Ref. [55].

#### B. Nonequilibrium molecular dynamics

For the nonequilibrium simulations, we used a variant of the boundary-driven nonequilibrium MD method developed by Ikeshoji and Hafskjold [56]. A liquid slab was placed in the middle of a rectangular simulation volume. We used  $10^5$  particles and the simulation-volume had dimensions  $\{L_x, L_y, L_z\} = \{40d, 40d, 200d\}$ . The temperature gradient was imposed in the  $z$  direction by thermostating the region  $|z/L_z| < 0.05$  to a low temperature  $T_c^*$ , and the regions  $0.45 < |z/L_z| < 0.5$  to a high temperature  $T_h^* = T_c^* + 0.5$  (in reduced units) with

the Langevin thermostat. At steady state (i.e., with zero mass flux), the heat flux,  $J_q$ , was constant and could be obtained from the kinetic energy absorbed or desorbed in the thermostats. The local thermal resistivity was defined by the following equation:

$$J_q = -\lambda(z) \frac{\partial T(z)}{\partial z} = -\frac{1}{r_k(z)} \frac{\partial T(z)}{\partial z}, \quad (24)$$

where  $\lambda$  is the local thermal conductivity and  $r_k$  is the local thermal resistivity to heat transfer. We calculated the local thermal resistivity by using Eq. [24], and the value of  $J_q$  and  $\frac{\partial T(z)}{\partial z}$  from the NEMD simulations. Moreover, the boundaries of the interfacial region as well as the surface temperature were calculated as described in previous work [57,58].

## IV. RESULTS

### A. Anisotropy in the spatial contributions to the configurational temperature

#### 1. Extended square gradient theory

To study the different contributions to the temperature in Eq. (17) with extended SGT, we solved the coupled differential equations defining the extended SGT framework [Eqs. (8)–(10)] to a relative accuracy of  $10^{-7}$ . Here, the cubic Peng-Robinson equation of state was used to describe the thermodynamic properties of the homogeneous fluid of argon [the terms with subscript 0 in Eqs. (8)–(10)] [59]. Different choices of influence parameters were evaluated, where all the choices reproduced the surface-tension of argon at 102 K [60]. In addition, by requiring the extended SGT to reproduce the maximum magnitude of  $\xi_{\perp}(z)$  from MD simulations, i.e.,  $\xi_{\text{md}(c),\perp}(z_T) = \xi_{\text{sgt}(c),\perp}(z_T)$ , resulted in the coefficients  $\kappa_{\rho} = 5.97 \times 10^{-15}$  Jm<sup>5</sup>/kmol<sup>2</sup>,  $\kappa_s = 3.5 \times 10^{-24}$  K<sup>2</sup>m<sup>5</sup>/J and a cross influence parameter equal to zero. We also explored the possibility of having a nonzero cross-coefficient,  $\kappa_{\rho s}$ . Using a nonzero cross-coefficient according to the geometric mean,  $\kappa_{\rho s} = \sqrt{\kappa_{\rho} \kappa_s}$ , resulted in contributions to the configurational temperature with a wavelet-like behavior, but with the opposite amplitudes compared to the MD-simulations. We found that the reason for this was that the gradients of the mass densities and the gradient of the configurational entropy density have the opposite sign across vapor-liquid interfaces. For SGT to give predictions which qualitatively agree with results from the MD simulations,  $\kappa_{\rho s}$  should be close to zero.

For the configurational temperature, the contributions from the directions parallel and perpendicular to the interface were found to differ, both in theory and simulations. We have plotted Eqs. (19) and (20) from the extended SGT-model as functions of position across the interface in Fig. 1 (left). The theory predicts that the perpendicular contribution to the temperature,  $\xi_{(c),\perp}(z)$ , has a wavelet-like behavior with a positive maximum at the vapor-side of the equimolar surface. The parallel contribution,  $\xi_{(c),\parallel}(z)$ , exhibits the opposite behavior with a maximum at the liquid-side. Changing the magnitude of the influence parameter  $\kappa_s$ , changed the amplitude of the wavelets, but kept their qualitative behavior unchanged.

#### 2. Molecular dynamics simulations

We performed standard MD simulations with constant total volume and number of particles as described in Sec. III

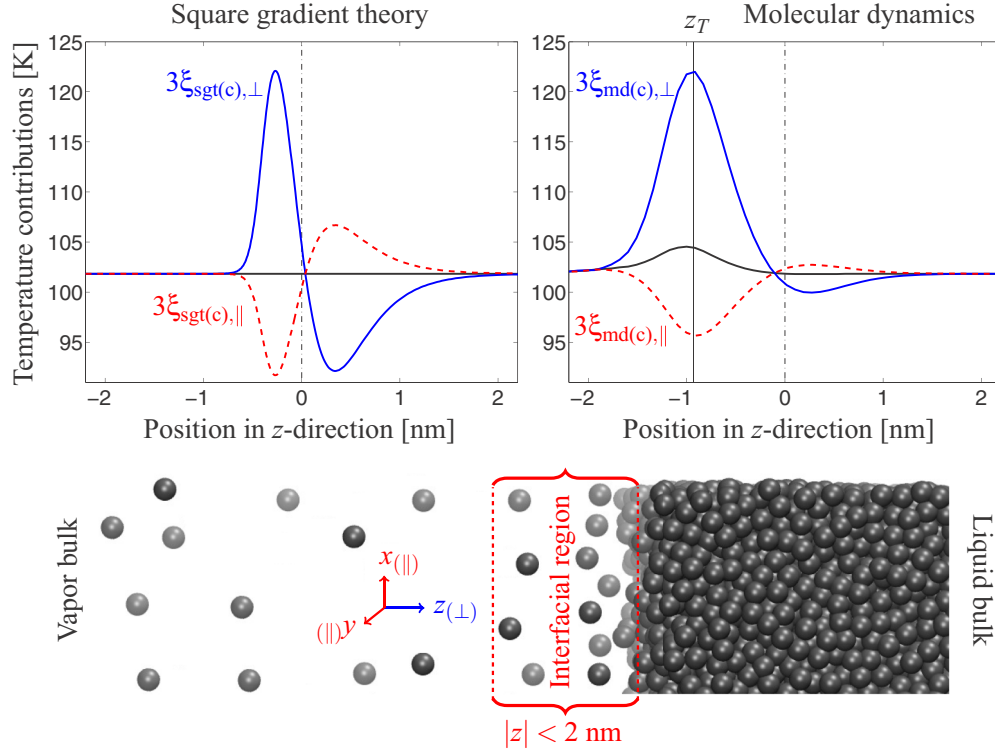


FIG. 1. (Top) A zoom-in at the interfacial region, showing the spatial contributions to the configurational temperatures perpendicular ( $\xi_{\perp}$ ) and parallel ( $\xi_{\parallel}$ ) to the vapor-liquid interface of argon/LJ-fluid at equilibrium ( $T = 102$  K,  $T^* = 0.85$ ). The left figure plots Eqs. (19) and (20) using results from extended SGT and the right figure plots the terms in Eq. (23) using results from MD with  $\xi_{\parallel} = (\xi_x + \xi_y)/2$ . The vertical dash-dot line shows the position of the equipmolar surface and the horizontal solid line, the system temperature. The vertical solid line shows the position of maximum temperature anisotropy,  $z_T$ . Vapor is located at  $z < -2$  and liquid at  $z > 2$ . (Bottom) Simulation snapshot illustrating the different regions (vapor, interface, and liquid bulk) and directions in space.

and computed the spatial contributions to the configurational temperature defined in Eq. (23). In Fig. 1 (right), they are plotted as functions of position across the interface. The figure displays a qualitative agreement between the theory [Fig. 1 (left)] and the analogous profiles from the MD simulations [Fig. 1 (right)]. Both theory and simulations give the same waveletlike behavior, where the perpendicular contribution has a maximum at the vapor-side and a minimum at the liquid-side of the equipmolar surface (vertical dash-dot line). In Fig. 2, we show that by using the same constant influence parameters as in Fig. 1, there is still a qualitative agreement at other temperatures as well, ranging from the triple point of argon to close to the critical point. In particular, both simulations and theory give that the extent of temperature anisotropy increases with decreasing temperature.

For the kinetic temperature, the spatial contributions across the interface from the MD simulations [Eq. (22)] have been plotted in Fig. 3. Here, the perpendicular and parallel contributions are the same. This is in agreement with the theory presented in Sec. II; in particular, the results from the MD simulations support the assumption in Eq. (6) that only the configurational part of the entropy density gives nonlocal contributions to the internal energy functional. We interpret the different behavior of the spatial contributions to the kinetic and configurational temperatures as a reflection of the fact that they represent complementary parts of the information contained in

the actual temperature of the system, where the temperature as defined in classical thermodynamics is based on the *total entropy* and the *total internal energy*.

### 3. Differences between theory and simulations and finite-size effects

Figure 1 displays a qualitative agreement between theory and simulations, but there are some differences. Most notably, the magnitude of the temperature anisotropy from the MD simulations is much more pronounced at the vapor-side. This suggests that the extended SGT theory derived in Sec. II has potential for improvement. To obtain predictions similar to the MD simulations, it is necessary to implement a more sophisticated version of extended square gradient theory, where the influence parameters,  $\kappa_{\rho}$  and  $\kappa_s$ , are functions of the densities.

It is well known that interfacial properties from molecular simulations depend strongly on both truncation distance and system size [61–63]. Mecke and Winkelmann showed that a sufficiently long truncation distance and tail corrections were necessary to obtain the surface tension of the full LJ potential to a high accuracy [61]. The surface width displays a particularly strong dependence on system size [64]. For the system size considered in our MD simulations however, Malfreyt showed that the size dependence can be neglected [63]. We showed in previous work how tail corrections are also needed for the configurational temperature at low truncation

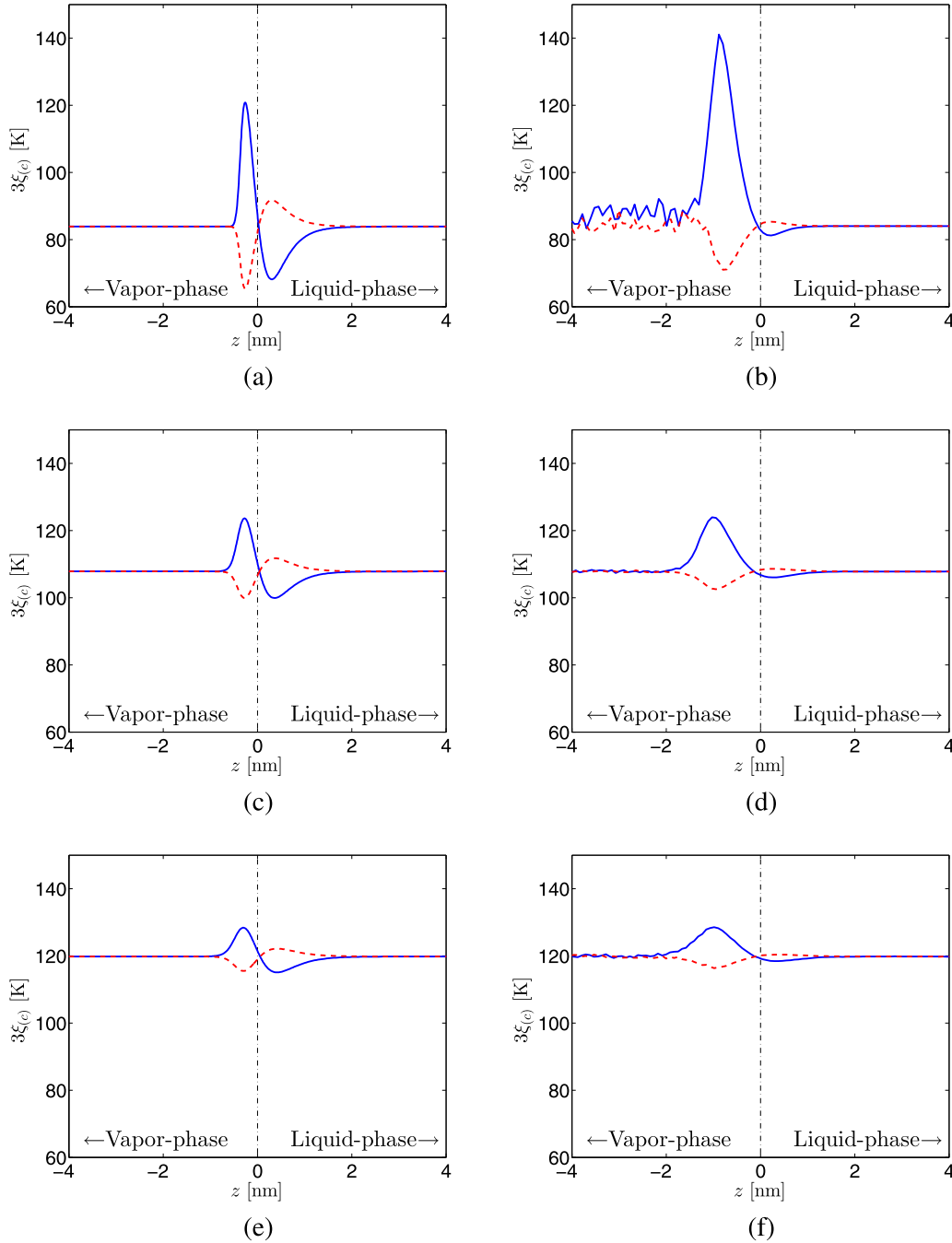


FIG. 2. The spatial contributions to the configurational temperatures perpendicular,  $\xi_{\perp}$  (blue solid lines), and parallel,  $\xi_{\parallel}$  (red dashed lines), to the vapor-liquid interface of argon *at equilibrium* at different temperatures. The figures to the left (a, c, e) show results from extended SGT and the figures to the right (b, d, f) show results from MD at  $T = 84$  K,  $T^* = 0.7$  (a, b),  $T = 108$  K,  $T^* = 0.9$  (c, d) and  $T = 120$  K,  $T^* = 1$  (e, f). The vertical dash-dot lines show the position of the equipolar surface.

distances [52], but such corrections can safely be neglected for the truncation distance used in this work (4d). In the following, we shall demonstrate that finite-size effects influence also the parallel and perpendicular contributions to the configurational temperature.

According to classical thermodynamics, the temperature at equilibrium should be constant in space,  $T(z) = T$ . This is in agreement with the theory derived in Sec. II. In the MD simulations, we find that the configurational temperature is constant and equal to the equilibrium temperature except in a

narrow region at the vapor-side of the equipolar surface, where  $T_{\text{md}(c)}$  exhibits a small positive deviation from  $T$  as shown in Fig. 1. The maximum amplitude of this deviation is located at  $z_T$  and is similar in size to the temperature-fluctuations in the vapor-phase. The deviation was also found in previous work [51]. We find that the deviation decreases monotonically with system size and is likely to be a consequence of the methodology used to calculate  $T_{\text{md}(c)}$  in the MD-simulations (see Sec. III), which suffers from the small number of particles in the bin,  $N_{\text{bin}}$  at the vapor-side of the equipolar surface.

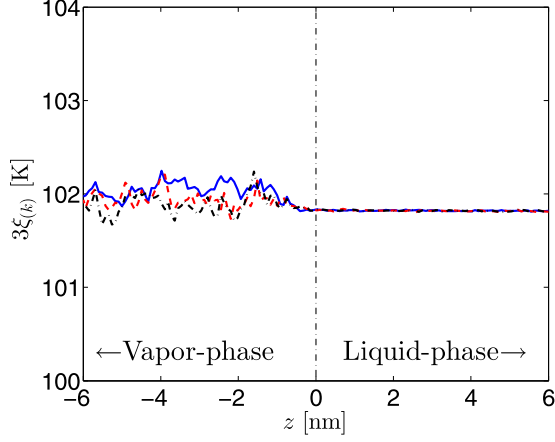


FIG. 3. The spatial contributions to the kinetic temperature defined in Eq. (22) from the direction perpendicular,  $\xi_{\text{md}(k),\perp}(z)$  (blue solid line), and parallel,  $\xi_{\text{md}(k),\parallel}(z)$  (red dashed and black dash-dot lines), to the vapor-liquid interface of argon at equilibrium at  $T = 102$  K,  $T^* = 0.85$ .

In agreement with previous work [51,52], we find that the fluctuations in the configurational temperature are larger than the fluctuations in the kinetic temperature.

We carried-out an in-depth analysis of the difference between  $T_{\text{md}(c)}$  and  $T$ , i.e., the accuracy of which  $T_{\text{md}(c)}$  can be obtained by using the methodology described in Sec. III. By performing  $NVE$ -simulations as described in Sec. III A with varying cross-section area ( $L_x L_y$ ) and thus varying number of particles in each bin  $N_{\text{bin}}$ , we found that the magnitude of  $T_{\text{md}(c)}(z_T) - T$  decreased monotonically with increasing number of particles in the bin and that the spatial contributions depended on system-size according to the following power laws:

$$\xi_{(c),\perp}(z) = \xi_{(c),\perp}^{\infty}(z) + k_{\perp}(z)N_{\text{bin}}^{-n}, \quad (25)$$

$$\xi_{(c),\parallel}(z) = \xi_{(c),\parallel}^{\infty}(z) + k_{\parallel}(z)N_{\text{bin}}^{-n}, \quad (26)$$

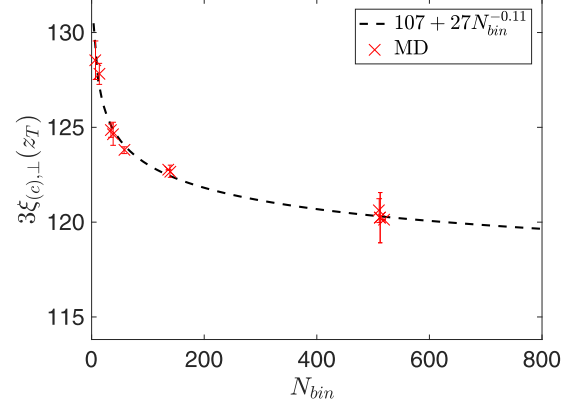
$$T_{(c)}(z) = T_{(c)}^{\infty}(z) + (2k_{\parallel}(z) + k_{\perp}(z))N_{\text{bin}}^{-n}, \quad (27)$$

where  $k_{\perp}(z)$  and  $k_{\parallel}(z)$  were spatially dependent parameters and  $n$  was a positive constant. We found that a single value for  $n$  was sufficient to account for all of the contributions in Eqs. (25)–(27). An unconstrained optimization routine was used to identify the parameters at  $z_T$  that minimized the least square distance between the MD results and the predictions from Eqs. (25)–(27). The resulting parameters are presented in the legends of Fig. 4.

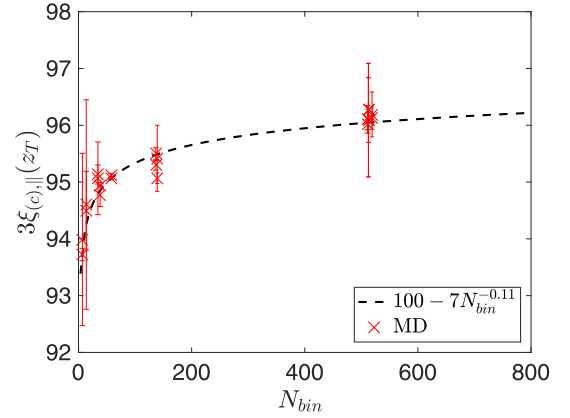
Figure 4 plots  $\xi_{\text{md}(c),\perp}$ ,  $\xi_{\text{md}(c),\parallel}$ , and  $T_{\text{md}(c)}$  as functions of  $N_{\text{bin}}$ . The figure shows that the resulting functions reproduce the MD results to a good accuracy. Two important conclusions can be made on the basis of the analysis:

(1) Eq. (27) fitted by an unconstrained optimization routine to match the MD results gives that  $T_{\text{md}(c)}^{\infty}(z_T) = T$ , showing that the inaccuracy in the methodology described in Sec. III vanishes in the limit of an infinitely large simulation volume.

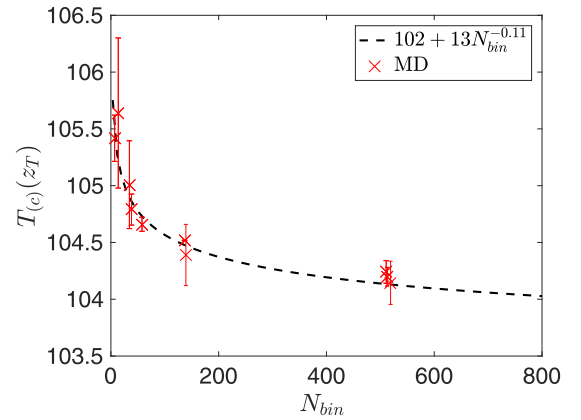
(2) In an infinitely large simulation volume, Eqs. (25) and (26) give that  $3\xi_{\text{md}(c),\perp}(z_T) \neq 3\xi_{\text{md}(c),\parallel}(z_T) \neq T$ , thus showing



(a)



(b)



(c)

FIG. 4. The magnitude of the spatial contributions (a, b) and the configurational temperature (c) in equilibrium MD simulations with  $T = 102$  K,  $T^* = 0.85$  as a function of the number of particles in the bin at  $z_T$  [see Fig. 1 from MD simulations (red crosses)] and as predicted by Eqs. (25)–(27) with parameters fitted to minimize the least square distance between the MD-results and the equations. The bin-width and  $L_z$  were kept unchanged, and  $N_{\text{bin}}$  was changed by modifying  $N$ ,  $L_x$ , and  $L_y$ .

that the anisotropy in the configurational temperature is also present in an infinitely large simulation volume.

The coefficients in the power laws presented in the legends of Fig. 4, reveal why  $T_{\text{md}(c)}$  exhibits a positive deviation from  $T$



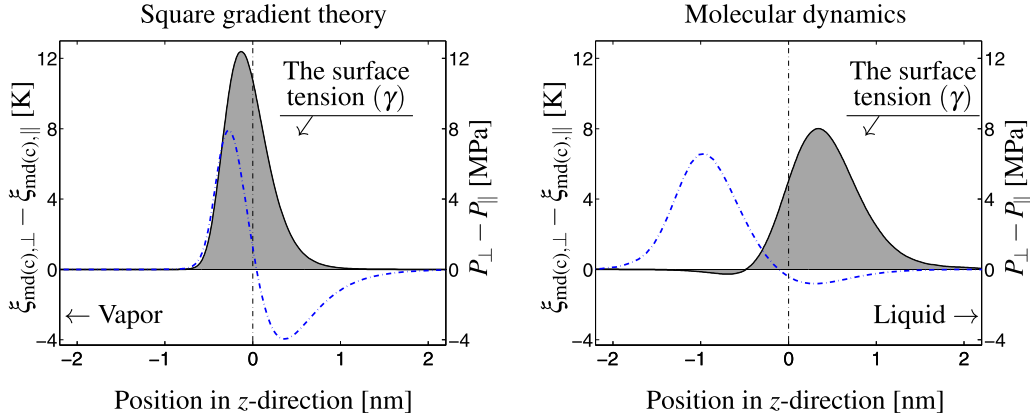


FIG. 5. The difference between the spatial contributions to the temperature (blue dash dot line) and the parallel and perpendicular components of the pressure tensor (solid line). The surface tension equals the integral given by the shaded area. The results come from extended SGT-theory or MD simulations at equilibrium at  $T = 108$  K,  $T^* = 0.9$  as described in Sec. III. Bulk vapor is at negative values of  $z$  and bulk liquid is at positive values of  $z$ .

at  $z_T$ . The coefficient  $k_{\perp}(z)$  is larger than  $-2k_{\parallel}(z)$ . This means that finite-size effects in the computation methodology have a stronger influence on the perpendicular contribution than the parallel contributions, which causes a small positive difference between  $T_{\text{md}(c)}$  and  $T$ .

### B. The influence of nonlocal entropic contributions on the equilibrium properties of interfaces

The qualitative agreement between theory and simulations displayed in Figs. 1 and 2 shows that nonlocal entropic contributions are likely to play a role in the thermodynamic description of interfaces. The only other thermodynamic properties that have been documented to be anisotropic across the planar vapor-liquid interface at equilibrium are the components of the pressure tensor,  $p_{\perp}(z)$  and  $p_{\parallel}(z)$ . The surface tension,  $\gamma$  can be obtained by integrating,  $p_{\perp}(z) - p_{\parallel}(z)$ , across the interface, illustrated by the shaded area in Fig. 5.

Figure 5 shows that the components of the pressure tensor behave fundamentally differently than  $\xi_{\perp}(z)$  and  $\xi_{\parallel}(z)$ . For the planar interface, we find that the perpendicular component of the pressure tensor,  $p_{\perp}(z)$  is constant and equal to the coexistence pressure. In MD simulations [Fig. 5 (right)], the difference,  $p_{\perp}(z) - p_{\parallel}(z)$ , has a maximum at the liquid-side of the equimolar surface (vertical dash-dot line). On the contrary, the difference,  $\xi_{(c),\perp}(z) - \xi_{(c),\parallel}(z)$ , has a maximum at the vapor-side of the equimolar surface. The corresponding quantities as predicted by extended SGT are shown in Fig. 5 (left). Here, the difference,  $p_{\perp}(z) - p_{\parallel}(z)$ , displays a maximum at the vapor-side of the equimolar surface (vertical dash-dot line).

A striking difference between SGT and MD-simulations is that  $p_{\perp}(z) - p_{\parallel}(z)$  displays a negative dip in MD-simulations [see Fig. 5 (right)], while it is always positive according to SGT [see Fig. 5 (left)]. The negative dip as well as the shift of the maximum in  $p_{\perp}(z) - p_{\parallel}(z)$  toward the liquid side of the equimolar surface observed in MD simulations can be reproduced by using more sophisticated density functional theory formulations (see, for instance, Fig. 6 in Ref. [65]). This elucidates the shortcomings of SGT and suggests that by including the entropy density as additional variable in a more sophisticated density functional theory formulation, it

would also be possible to reproduce the shift of the maximum in  $\xi_{(c),\perp}(z) - \xi_{(c),\parallel}(z)$  toward the vapor-side of the equimolar surface. This represents important future work.

In Fig. 1, we chose the influence parameters such that the theory reproduces the surface tension of argon at  $T = 102$  K and so that  $\xi_{\text{sgt}(c),\perp}(z_T) = \xi_{\text{md}(c),\perp}(z_T)$ . For this choice of influence parameters, nonlocal entropic contributions are responsible for about 17% of the total magnitude of the surface tension. This indicated that nonlocal entropic contributions are of a similar magnitude as the terms from the classical theory, although 17% is probably a too high estimate. Even though the extended SGT gives a temperature anisotropy that follows the MD simulations reasonably well at the vapor side, the extent of anisotropy at the liquid side is systematically over predicted (See Fig. 2). Moreover, the finite-size effects that come from the computational methodology discussed in Sec. IV A 3 will lead to a further decrease in the magnitude of the nonlocal entropic contributions in comparison to Fig. 1 (see Fig. 4). We find that the terms in Eq. (13) that come from nonlocal entropic contributions exhibit a different behavior than the terms from the classical theory and influence both the predicted temperature and curvature dependence of the surface tension. Since the extended SGT presented in Sec. II is unable to reproduce the profiles from MD simulation quantitatively, an accurate assessment of the magnitude of the nonlocal entropic contributions and their influence on the temperature dependence of the surface tension represents future work.

### C. A link between the temperature anisotropy at equilibrium and the Kapitza resistance at nonequilibrium

We shall next discuss a possible connection between the nonlocal entropic contributions missing from the classical theory and the transport properties of the interface at nonequilibrium.

Figure 1 (right) and Fig. 2 demonstrate that the extent of temperature anisotropy from simulations is much more pronounced at the vapor-side of the equimolar surface where  $\xi_{\text{md}(c),\perp} - \xi_{\text{md}(c),\parallel}$  displays a maximum at  $z_T$ . No other equilibrium property has so far been documented to display a similar preference for the vapor-phase across the vapor-liquid

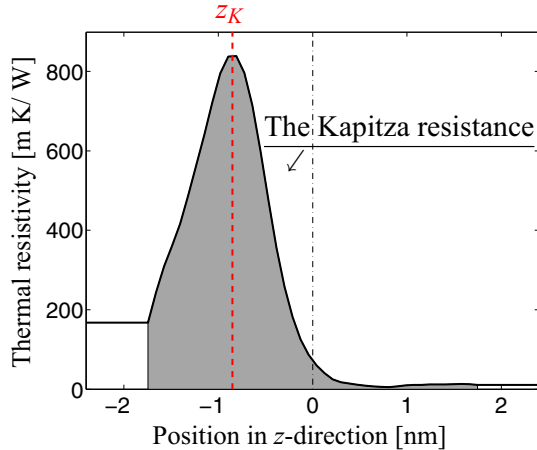


FIG. 6. The thermal resistivity across the interface obtained from NEMD simulations using the methodology described in Sec. III, where the temperature of the cold thermostat was  $T_c = 108$  K,  $T^* = 0.9$ . The shaded area gives the Kapitza resistance.

interface. At nonequilibrium on the other hand, it has for long been known that the characteristic temperature jump across the vapor-liquid interface is located at the vapor side of the equimolar surface [10,11,35,66]. By performing nonequilibrium molecular dynamics simulations (NEMD) as explained in Sec. III, we find that the thermal resistivity (the reciprocal thermal conductivity) exhibits a behavior that is remarkably similar to the temperature anisotropy. This is evident by comparing Fig. 1 (right) with Fig. 6. Since the Kapitza resistance can be obtained by integrating the local thermal resistivity across the interfacial region, the shaded area in Fig. 6, the thermal resistivity represents its local structure.

Similar to the temperature anisotropy, the thermal resistivity has a maximum at the vapor side of the equimolar surface, located at  $z_K$ . We find that  $z_K$  obtained from nonequilibrium simulations matches almost perfectly with  $z_T$  obtained from equilibrium simulations when plotted as a function of the surface temperature [57]. Both maxima follow the red dashed line in Fig. 7, positioned  $\sim 1$  nm into the vapor side relative to the equimolar surface. This links the anisotropy in the configurational part of the temperature under *equilibrium* conditions to the Kapitza resistance observed under *nonequilibrium* conditions.

Since nonlocal entropic contributions give a qualitative explanation for the temperature anisotropy found at equilibrium (see Fig. 1), they are also likely to play a role in the theoretical description of the Kapitza resistance of the vapor-liquid interface, a description that is currently missing [35]. The theory that links these properties remains to be developed. Such a theory is important because it provides the means for using SGT to estimate not only the surface tension, but also the rates at which heat and mass are transferred across interfaces at nonequilibrium by taking advantage of the so-called integral relations [9]. At present, a semiempirical fit of the local thermal resistivity function is required to obtain the transport properties of the interface with SGT. This was accomplished in Ref. [37] for both planar and curved interfaces of the LJ-fluid by combining NEMD and a semi-empirical SGT formulation. Here,

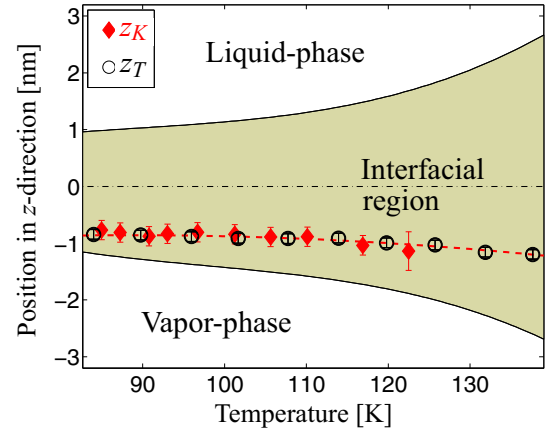


FIG. 7. Position of the maximum of the temperature anisotropy,  $z_T$ , and the maximum of the thermal resistivity,  $z_K$ , plotted as functions of the surface temperature for argon/the LJ fluid. The shaded area is the interfacial region, where the solid lines and the surface temperature have been calculated using the approach of Xu *et al.* in Ref. [57].

the maximum of the local thermal resistivity was allocated to the vapor-side of the equimolar surface by invoking an inverse density dependence [11]. Rather than fitting this function, a long-term aim should be to develop a predictive theory for the local thermal resistivity across interfaces. Figure 7 suggests that nonlocal entropic contributions will play a role in such a description.

## V. CONCLUSION

In this work, we have revisited the fundamentals of density gradient theory. Rather than using the Helmholtz energy as starting point like in the classical theory, we have used the internal energy with the entropy density as additional variable. The extended theory then suggests that the configurational temperature has different contributions from the parallel and perpendicular directions at the interface and that the kinetic temperature has equal contributions.

We evaluated these predictions by use of standard molecular dynamics simulations at constant total energy and volume and obtained behaviors of the spatial contributions to the configurational and kinetic temperatures that were in qualitative agreement with the extended theory. The extended theory showed that the anisotropy in the configurational temperature originates in nonlocal entropic contributions, which are currently missing from the classical theory. Nonlocal entropic terms enter the expression for the tension tensor and influence thus the predicted surface tension. Since the nonlocal entropic terms behave differently than the classical terms, they are likely to influence both the temperature- and curvature-dependence of the surface tension and may account for part of the discrepancy between experiments and theory.

For a particular choice of influence parameters that reproduced certain characteristics of the simulations results, it was shown that nonlocal entropic contributions were responsible for about 17% of the total magnitude of the surface tension. Nonlocal entropic contributions are thus of a similar magnitude

as the classical terms, although 17% is probably a too high estimate. Further development of the theory is necessary to reproduce the results from MD quantitatively and to provide a reliable evaluation of the significance of nonlocal entropic terms.

The thermal resistivity gives the local structure of the interfacial resistance to heat transfer, where the integral gives the Kapitza resistance. Across the vapor-liquid interface of the LJ-fluid, we found that the maximum in the temperature anisotropy at equilibrium coincided precisely with the maximum in the thermal resistivity at nonequilibrium relative to the equimolar surface, when plotted as a function of the surface temperature. The similarity between the temperature anisotropy and the thermal resistivity is striking and strongly suggests that nonlocal entropic contributions may play a role in the theoretical description of the Kapitza resistance of the

vapor-liquid interface. However, the theory that links these properties remains to be developed. Such a theory is important because it provides the means for using SGT to estimate not only the surface tension, but also the rates at which heat and mass are transferred across interfaces at nonequilibrium by taking advantage of the so-called integral relations.

#### ACKNOWLEDGMENTS

The authors thank Signe Kjelstrup, Dick Bedeaux, Titus S. van Erp, and David Reguera for fruitful discussions and Magnus Waage for useful comments to the manuscript. The computational resources were granted by The Norwegian Metacenter for Computational Science (NOTUR) Project No. nn9229k.

- 
- [1] J. A. Huberman and A. D. Riggs, *J. Mol. Biol.* **32**, 327 (1968).  
 [2] D. R. Baker, F. Brun, C. O'Shaughnessy, L. Mancini, J. L. Fife, and M. Rivers, *Nat. Commun.* **3**, 1135 (2012).  
 [3] M. Kulmala, H. Vehkamäki, T. Petäjä, M. Dal Maso, A. Lauri, V. M. Kerminen, W. Birmili, and P. H. McMurry, *J. Aerosol Sci.* **35**, 143 (2004).  
 [4] J. S. Rowlinson and B. Widom, *Molecular Theory of Capillarity* (Clarendon Press, Oxford, 1984).  
 [5] E. M. Blokhuis and A. E. van Giessen, *J. Phys.: Condens. Matter* **25**, 225003 (2013).  
 [6] Z. Li and J. Wu, *Ind. Eng. Chem. Res.* **47**, 4988 (2008).  
 [7] B. J. Block, S. K. Das, M. Oettel, P. Virnau, and K. Binder, *J. Chem. Phys.* **133**, 154702 (2010).  
 [8] A. Tröster, M. Oettel, B. Block, P. Virnau, and K. Binder, *J. Chem. Phys.* **136**, 064709 (2012).  
 [9] S. Kjelstrup and D. Bedeaux, *Nonequilibrium Thermodynamics of Heterogeneous Systems* (World Scientific, Singapore, 2008).  
 [10] Ø. Wilhelmsen, D. Bedeaux, and S. Kjelstrup, *Phys. Chem. Chem. Phys.* **16**, 10573 (2014).  
 [11] Ø. Wilhelmsen, T. T. Trinh, S. Kjelstrup, T. S. van Erp, and D. Bedeaux, *Phys. Rev. Lett.* **114**, 065901 (2015).  
 [12] Ø. Wilhelmsen, T. T. Trinh, A. Lervik, V. K. Badam, S. Kjelstrup, and D. Bedeaux, *Phys. Rev. E* **93**, 032801 (2016).  
 [13] H. Lin, Y.-Y. Duan, and Q. Min, *Fluid Phase Equilib.* **254**, 75 (2007).  
 [14] J. Gross, *J. Chem. Phys.* **131**, 204705 (2009).  
 [15] G. P. Morriss and L. Rondoni, *Phys. Rev. E* **59**, R5 (1999).  
 [16] J. G. Powles, G. Rickayzen, and D. M. Heyes, *Mol. Phys.* **103**, 1361 (2005).  
 [17] J. Dunkel and S. Hilbert, *Nat. Phys.* **10**, 67 (2014).  
 [18] J. M. G. Vilar and J. M. Rubi, *J. Chem. Phys.* **140**, 201101 (2014).  
 [19] D. Frenkel and P. B. Warren, *Am. J. Phys.* **83**, 163 (2015).  
 [20] V. K. Badam, V. Kumar, F. Durst, and K. Danov, *Exp. Thermal Fluid Sci.* **32**, 276 (2007).  
 [21] W. C. Moss, D. B. Clarke, and D. A. Young, *Science* **276**, 1398 (1997).  
 [22] A. Bass, S. J. Ruuth, C. Camara, B. Merriman, and S. Putterman, *Phys. Rev. Lett.* **101**, 234301 (2008).  
 [23] D. J. Flannigan and K. S. Suslick, *Nat. Phys.* **6**, 598 (2010).  
 [24] J. M. Simon and J. M. Rubi, *J. Phys. Chem. B* **115**, 1422 (2011).  
 [25] J. C. Barrett, *J. Chem. Phys.* **135**, 096101 (2011).  
 [26] J. W. P. Schmelzer, G. S. Boltachev, and A. S. Abyzov, *J. Chem. Phys.* **139**, 034702 (2013).  
 [27] M. Schweizer and L. M. C. Sagis, *J. Chem. Phys.* **141**, 224102 (2014).  
 [28] P. Keblinski, S. R. Phillpot, S. U. S. Choi, and J. A. Eastman, *Int. J. Heat Mass Transfer* **45**, 855 (2002).  
 [29] H. E. Patel, S. K. Das, T. Sundararajan, A. S. Nair, B. George, and T. Pradeep, *Appl. Phys. Lett.* **83**, 2931 (2003).  
 [30] H. A. Patel, S. Garde, and P. Keblinski, *Nano Lett.* **5**, 2225 (2005).  
 [31] Z. Ge, D. G. Cahill, and P. V. Braun, *Phys. Rev. Lett.* **96**, 186101 (2006).  
 [32] C. Cheng, W. Fan, J. Cao, S.-G. Ryu, J. Ji, C. P. Grigoropoulos, and J. Wu, *ACS Nano* **5**, 10102 (2011).  
 [33] Z. Liang, K. Sasikumar, and P. Keblinski, *Phys. Rev. Lett.* **113**, 065901 (2014).  
 [34] H.-K. Lyee and D. G. Cahill, *Phys. Rev. B* **73**, 144301 (2006).  
 [35] M. Bond and H. Struchtrup, *Phys. Rev. E* **70**, 061605 (2004).  
 [36] J. Ge, S. Kjelstrup, D. Bedeaux, J. M. Simon, and B. Rousseau, *Phys. Rev. E* **75**, 061604 (2007).  
 [37] Ø. Wilhelmsen, T. T. Trinh, S. Kjelstrup, and D. Bedeaux, *J. Phys. Chem. C* **119**, 8160 (2015).  
 [38] J. F. Lutsko, *J. Chem. Phys.* **134**, 164501 (2011).  
 [39] R. Evans, *Fundamentals of Inhomogeneous Fluids* (Marcel Dekker, New York, 1992), Chap. 3.  
 [40] R. Roth, *J. Phys.: Condens. Matter* **22**, 063102 (2010).  
 [41] H. B. Callen, *Thermodynamics and an Introduction to Thermostatistics* (John Wiley & Sons, New York, 1985).  
 [42] D. W. Oxtoby, *Annu. Rev. Mater. Res.* **32**, 39 (2002).  
 [43] H. Löwen, *J. Phys. Condens. Matter* **14**, 11897 (2002).  
 [44] J. Wu and Z. Li, *Annu. Rev. Phys. Chem.* **58**, 85 (2007).  
 [45] K. Huang, *Statistical Mechanics* (John Wiley and Sons, New York, 1963).  
 [46] G. H. A. Cole, *An Introduction to the Statistical Theory of Classical Simple Dense Fluids* (Pergamon Press, Oxford, 1967).  
 [47] J. W. Cahn and J. E. Hilliard, *J. Chem. Phys.* **28**, 258 (1958).  
 [48] A. J. M. Yang, P. D. Fleming, and J. H. Gibbs, *J. Chem. Phys.* **64**, 3732 (1976).  
 [49] O. G. Jepps, G. Ayton, and D. J. Evans, *Phys. Rev. E* **62**, 4757 (2000).  
 [50] A. Lervik, Ø. Wilhelmsen, T. T. Trinh, and H. R. Nagel, *J. Chem. Phys.* **143**, 114106 (2015).

- [51] N. Jackson, M. Rubi, and F. Bresme, *Mol. Simul.* **42**, 1214 (2016).
- [52] A. Lervik, Ø. Wilhelmsen, T. T. Trinh, and E. M. Blokhuis, *J. Chem. Phys.* **144**, 056101 (2016).
- [53] S. Plimpton, *J. Comput. Phys.* **117**, 1 (1995).
- [54] L. A. Rowley, D. Nicholson, and N. G. Parsonage, *J. Comput. Phys.* **17**, 401 (1975).
- [55] T. Nakamura, S. Kawamoto, and W. Shinoda, *Comput. Phys. Commun.* **190**, 120 (2015).
- [56] T. Ikeshoji and B. Hafskjold, *Mol. Phys.* **81**, 251 (1994).
- [57] J. Xu, S. Kjelstrup, D. Bedeaux, A. Røsjorde, and L. Rekvig, *J. Colloid Interface Sci.* **299**, 452 (2006).
- [58] R. Rurali, L. Colombo, X. Cartoixa, Ø. Wilhelmsen, T. T. Trinh, D. Bedeaux, and S. Kjelstrup, *Phys. Chem. Chem. Phys.* **18**, 13741 (2016).
- [59] D. Y. Peng and D. B. Robinson, *Ind. Eng. Chem. Fundamen.* **15**, 59 (1976).
- [60] E. W. Lemmon and S. G. Penoncello, in *Advances in Cryogenic Engineering*, Vol. 39 (Springer, Boston, MA, 1994), pp. 1927–1934.
- [61] M. Mecke and J. Winkelmann, *J. Chem. Phys.* **107**, 9264 (1997).
- [62] A. Trokhymchuk and J. Alejandre, *J. Chem. Phys.* **111**, 8510 (1999).
- [63] P. Malfreyt, *Mol. Simul.* **40**, 106 (2014).
- [64] C. D. Holcomb, P. Clancy, and J. A. Zollweg, *Mol. Phys.* **78**, 437 (1993).
- [65] E. Johannessen, J. Gross, and D. Bedeaux, *J. Chem. Phys.* **129**, 184703 (2008).
- [66] J. M. Simon, D. Bedeaux, S. Kjelstrup, J. Xu, and E. Johannessen, *J. Phys. Chem. B* **110**, 18528 (2006).